symmetry

MDPI

Article

MoO_3 Interlayer Modification on the Electronic Structure of Co/BP Interface

Baoxing Liu [1,2], Haipeng Xie [1,*], Yuan Zhao [1], Dongmei Niu [1] and Yongli Gao [3]

[1] Hunan Key Laboratory for Super-Microstructure and Ultrafast Process, School of Physics and Electronics, Central South University, Changsha 410012, China
[2] College of Physics and Optoelectronic Engineering, Shenzhen University, Shenzhen 518060, China
[3] Department of Physics and Astronomy, University of Rochester, Rochester, NY 14627, USA
* Correspondence: xiehaipeng@csu.edu.cn

Abstract: The modification by molybdenum trioxide (MoO_3) buffer layer on the electronic structure between Co and black phosphorus (BP) was investigated with ultraviolet photoemission spectroscopy (UPS) and X-ray photoemission spectroscopy (XPS). It was found that the MoO_3 buffer layer could effectively prevent the destruction of the outermost BP lattice during the Co deposition, with the symmetry of the lattice remaining maintained. There is a noticeable interfacial charge transfer in addition to the chemical reaction between Co and MoO_3. The growth pattern of Co deposited onto the MoO_3/BP film is the island growth mode. The observations reveal the significance of a MoO_3 buffer layer on the electronic structure between Co and black phosphorus and provide help for the design of high-performance Co/BP-based spintronic devices.

Keywords: black phosphorus; molybdenum trioxide; Cobalt; buffer layer; photoemission spectroscopy

check for updates

Citation: Liu, B.; Xie, H.; Zhao, Y.; Niu, D.; Gao, Y. MoO_3 Interlayer Modification on the Electronic Structure of Co/BP Interface. *Symmetry* **2022**, *14*, 2448. https://doi.org/10.3390/sym14112448

Academic Editors: Xiaolei Wang, Xueyun Wang and Chao Shen

Received: 15 October 2022
Accepted: 14 November 2022
Published: 18 November 2022

Publisher's Note: MDPI stays neutral with regard to jurisdictional claims in published maps and institutional affiliations.

Copyright: © 2022 by the authors. Licensee MDPI, Basel, Switzerland. This article is an open access article distributed under the terms and conditions of the Creative Commons Attribution (CC BY) license (https://creativecommons.org/licenses/by/4.0/).

1. Introduction

Black phosphorus is a two-dimensional layered puckered material with unique crystal symmetry and has broad application prospects in electrical, optical, energy storage, and other fields [1–5]. In recent years, devices based on BP have emerged continuously, such as field effect transistors [6,7], infrared photodetectors [8–10], thin film solar cells [11,12], polarizers [13], gas sensors [14], etc. BP also has great potential for applications in new spintronic devices. Co is one of the most common ferromagnetic electrodes and is widely used for the injection and detection of spin-polarized currents in devices. Sui et al. applied density functional theory to study the properties of Co atoms adsorbed on BP and found that Co atoms can combine with BP with considerable binding energy [15]. The Co/BP system exhibits interesting magnetic properties due to the cross-splitting of Co 3d orbitals. Kamalakar et al. used TiO_2/Co as the contact electrode of the device to prepare a multilayer BP field effect transistor [16]. The test results showed that there was a magnetoresistance effect in the transistor.

Chirality has attracted a great deal of attention in recent decades for its applications in various disciplines such as polarization optics, spectroscopy, analytical chemistry, and molecular biology. External chirality can be realized in nonchiral anisotropic planar metamaterials, resulting from the mutual orientation of the metamaterial structure and the incident electromagnetic wave. Strong external chirality has been predicted to occur in BP because of its in-plane anisotropy [17].

The breakdown of bulk symmetry at surface and interfaces is of fundamental importance in many areas, including spintronics, ferroics and light–matter interactions. Furthermore, the morphology and electronic structure at the surface and interfaces can add rich physics that requires systematic and meticulous investigations. Although metals are used as electrode materials in many BP-based devices with various functions, the deposition

of metal will usually damage the BP. It finds that there have different influences on the metal/BP interface. There is a reaction between Al and BP [18], and the unique crystal symmetry structure will be destroyed in Co/BP and Au/BP interface [19,20], and so inserting a buffer layer at the interface is necessary. Semiconductor metal oxide thin films are widely used as buffer layer materials. Molybdenum trioxide is a promising semiconductor metal oxide as the active layer of gas sensors and photodetectors [21–25]. Xiang et al. used MoO_3 to modify BP, resulting in a huge hole-doping effect on BP field effect transistors [22]. With the increase of the doping thickness of MoO_3, the conductivity of the BP field effect transistor will be greatly improved.

The effect of MoO_3 buffer layer on the interface electronic structure of Co/BP interface has been studied by UPS and XPS. The results showed that the MoO_3 buffer layer can effectively prevent damage to the BP lattice caused by the metal deposition process. During the deposition process, there is an interfacial interaction between Co and MoO_3. The findings provide guidance for the development of spintronic devices based on Co/MoO_3/BP.

2. Experimental Method

All growth and test were carried out in a set of ultra-high vacuum interconnection systems at room temperature with vacuum pressures better than 1×10^{-9} mbar. In the preparation chamber, the BP crystal was mechanically peeled in a vacuum. Its quality was checked by XPS (SPECS XR-MF, Al Kα = 1486.7 eV) in the analysis chamber in order to ensure successful dissociation. UPS was tested by exciting sample with Specs Microwave UV Light Source (He I = 21.22 eV). The hemispherical energy analyzer used for XPS and UPS is SPECS PHPIBOS 150. For XPS measurement, the equipment was calibrated with clean polycrystalline Au. The X-ray source was operated at 100 W with 40 eV pass energy and 100 meV scanning steps for all tests. The XPS spectrum was fitted in detail with CasaXPS. The UPS measurements were performed with a -5 V bias applied to the sample. A total energy resolution was about 70 meV for the UPS as determined from the Fermi edge of clean Au (111). In the experiment, the Co film and MoO_3 film were grown by thermal evaporation, the growth thickness of the film was monitored by quartz crystal microbalance. The sample was transferred through the manipulator of the radial distribution chamber. The transfer step was under ultra-high vacuum environment, preventing sample contamination.

3. Results and Discussion

The crystal structure of BP is shown in Figure 1a, the atomic layers of BP are superimposed by weak van der Waals interaction. The interlayer distance is about 5 Å, and the lattice constants are a = 3.313 Å, b = 4.374 Å, and c = 10.473 Å, respectively [26]. Figure 1c is the XPS full spectrum of BP after dissociation, it can be seen that the P 2s and P 2p peaks of BP are located at 188.4 eV and 130.7 eV, respectively. No impurity peaks such as carbon and oxygen were found, indicating that the clean BP surface was successfully exfoliated. Figure 1b shows the MoO_3 lattice structure, where molybdenum atoms are represented by larger spheres and oxygen atoms are represented by smaller spheres [27]. The cuboid in the figure marks the octahedral MoO_6 cluster, which is the construction unit of MoO_3 crystal, and the lattice constants are a = 3.962 Å, b = 13.855 Å, c = 3.699 Å, respectively. Figure 1d shows the full XPS spectrum after depositing 3 nm MoO_3 on BP. No peaks of P 2s and P 2p were found, indicating that 3 nm MoO_3 would completely cover BP. Our previous research has shown that the growth process of MoO_3 is physical adsorption on BP, and the BP lattice will not be destroyed [18]. The O 1s and Mo $3d_{5/2}$ peaks are located at 530.5 and 232.7 eV, respectively, which are consistent with the previous test results, indicating that MoO_3 thin films were successfully grown [28].

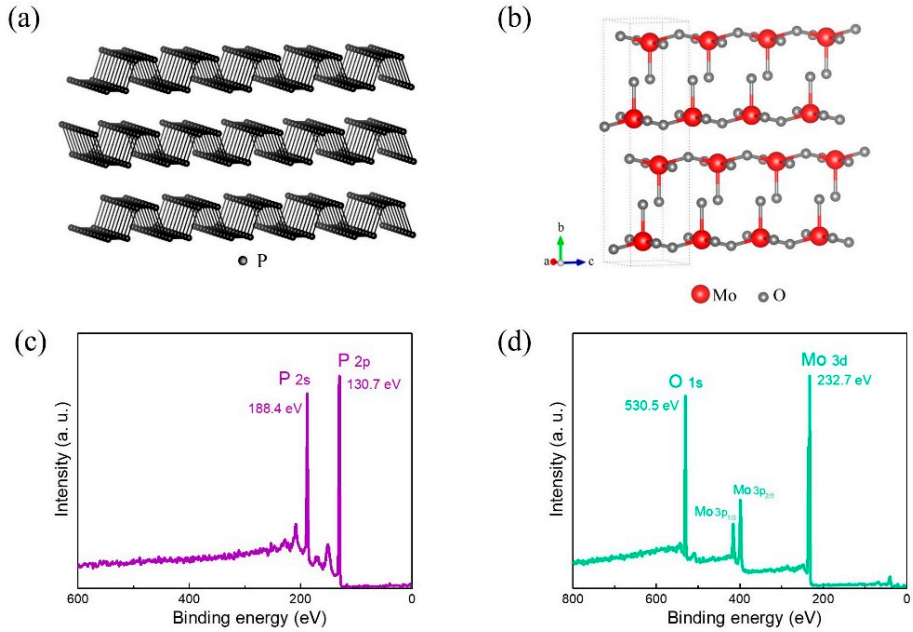

Figure 1. The crystal structure of (**a**) BP and (**b**) MoO_3. XPS full spectrum of (**c**) BP and (**d**) MoO_3.

Co thin films were grown on MoO3/BP and Figure 2 shows the UPS spectra as a function of Co film thickness. The work function (WF) is 4.24 eV and 6.33 eV for the intrinsic BP and MoO3 films, respectively. When 1 Å Co was deposited, the WF decreased to 5.34 eV, and continued to decrease with increasing Co thickness. After depositing 8 Å Co, the WF reaches a minimum of 4.89 eV with a shift of 1.44 eV. As the Co thickness continued to increase, the WF began to increase, and the WF of the Co/MoO3/BP film was 5.24 eV after 60 Å Co deposition. Figure 2b shows the UPS valence band region, the valence band maximum (VBM) of the intrinsic BP is ~0.1 eV. After depositing 3 nm MoO3 film, the VBM becomes 2.72 eV. The Fermi level in the figure is marked with a solid line. It can be seen that the Fermi edge of the metal begins to appear when the deposition thickness of Co is 8 Å. In the Co/BP interface, the Fermi edge of the metal begins to appear after the deposition of 4 Å Co. Comparing the UPS data of the Co/MoO3/BP interface and the Co/BP interface [19], it can be inferred that the chemical reaction between Co and MoO3 has been averted by inserting the MoO3 at the Co/BP interface, which delayed the emergence of the Fermi edge of metallic Co.

The XPS spectra as a function of Co thickness when growing Co thin films on MoO_3/BP is shown in Figure 3. When the thickness of Co is 1−4 Å, the Co 2p peak is located at 781.58 eV, corresponding to Cobalt oxide (CoO_x) [29,30]. At 8–15 Å, a new peak appears at 778.75 eV, corresponding to metallic Co. The appearance of CoO_x proves that there is a chemical reaction at the Co/MoO_3 interface. The O 1s and Mo 3d spectra were fitted in detail, the information is in Table S1. Figure 3b shows the fitted O 1s spectrum, the blue peak corresponds to the oxygen component in CoO_x, which is located at 531.45 eV. With the increase of Co thickness, the proportion of oxygen in CoO_x increases gradually. The red peak corresponds to the oxygen component in MoO_3, which is located at 530.51 eV. To further analyze the growth process of Co on MoO_3/BP films, we investigated the attenuation of XPS intensity by the capping layer. The attenuation curve of XPS intensity can be used to analyze the growth mode of the deposit on the substrate [31]. In the Co/MoO_3 interface, the intensity of photoelectrons emitted from Co 2p gradually decreases as the Co thickness increases from 0 to 8 Å. When the thickness is greater than 8 Å, the attenuation of photoelectrons by the Co coating increases significantly, which can be attributed to the island growth of Co. At lower Co coverage (Θ < 8 Å), Co atoms form clusters, which will expose more substrates than the uniformly distributed Co films. Hence the photoelectron intensity decreases slowly at the beginning, corresponding to the smaller

slope shown by the red dashed line in Figure 4b. When the Co covering layer has a sufficient thickness (Θ > 8 Å), the island clusters will be connected to each other to form a continuous covering layer, which will significantly increase the attenuation of photoelectrons. The corresponding slope also becomes larger. Therefore, it can be inferred that the growth mode of Co deposition on MoO_3/BP films is island growth.

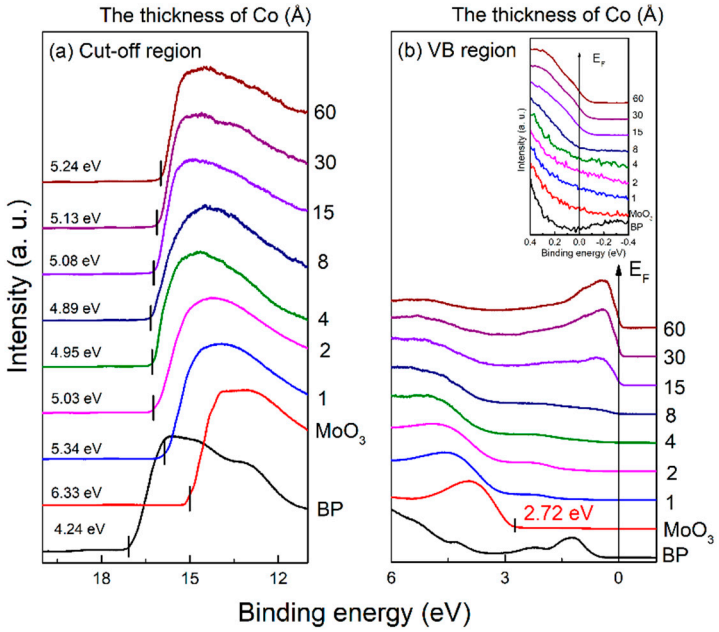

Figure 2. UPS spectra as a function of Co film thickness when growing Co thin films on MoO_3/BP, (**a**) cut−off region, (**b**) VB region, Inset: the locally enlarged view of the VB edge region near E_F.

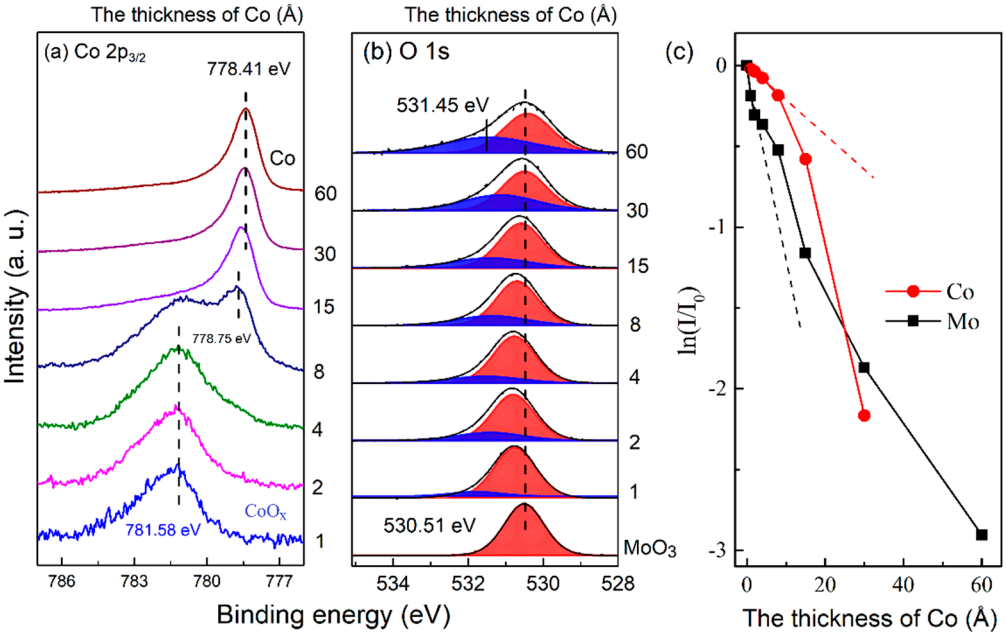

Figure 3. XPS spectra as a function of Co film thickness when growing Co thin films on MoO_3/BP. (**a**) Co 2p, (**b**) O 1s, the blue (red) peak corresponds to the oxygen component in CoO_x (MoO_3). (**c**) Photoelectron intensity as a function of Co film thickness. The red (black) dashed line marks the slope of Co 2p (Mo 3d) before Co deposition to 8 Å.

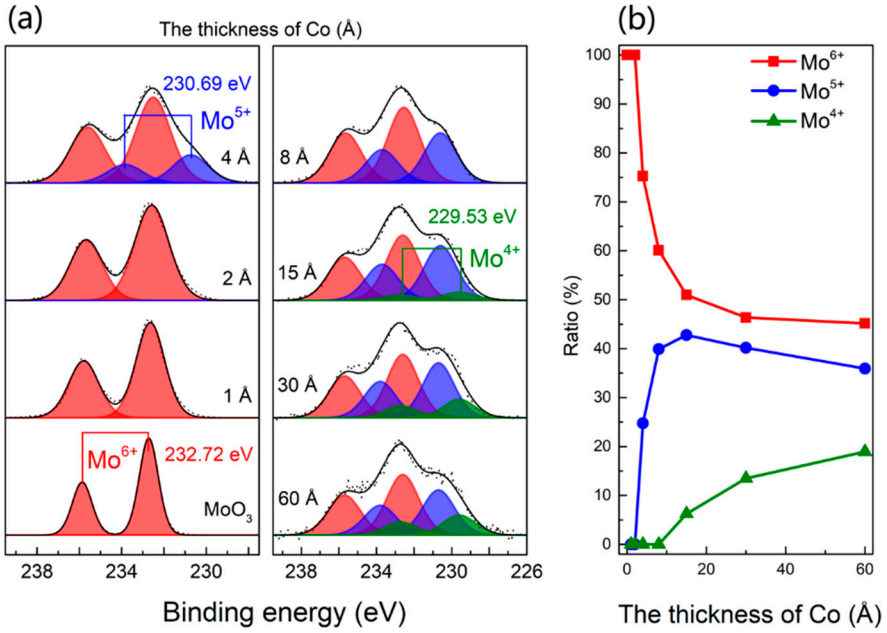

Figure 4. (**a**) Mo 3d spectra as a function of Co film thickness when growing Co thin films on MoO_3/BP. The red, blue, and green peaks are represented as Mo^{6+}, Mo^{5+}, Mo^{4+} oxidation states, respectively. (**b**) The proportion of different oxidation states of Mo varies with Co thickness.

The Mo 3d spectra as a function of Co film thickness when Co thin films deposition on MoO_3/BP is shown in Figure 4a. The Mo 3d peak consists of Mo $3d_{3/2}$ and Mo $3d_{5/2}$, for simplicity, here only discusses the Mo $3d_{5/2}$ peak. The different color peaks correspond to different oxidation states of Mo, the red, blue, and green peaks are represented as Mo^{6+}, Mo^{5+}, and Mo^{4+}, respectively. Their corresponding binding energies are, respectively, located at 232.72 eV, 230.69 eV, and 229.53 eV. In intrinsic MoO_3, the oxidation state of Mo is Mo^{6+}. The Mo^{5+} oxidation state appears when the deposition thickness of Co is 4 Å, and the Mo^{4+} oxidation state appears at 15 Å. The proportion of different oxidation states of Mo varies with Co thickness as shown in Figure 4b. From 1 to 15 Å, the proportion of the Mo^{6+} oxidation state decreases monotonously from 100% to 50%. The Mo^{5+} oxidation state first increases and then decreases with the increase of Co thickness, reaching a maximum value of 43% at 15 Å. The Mo^{4+} oxidation state increases monotonically with the Co thickness, and the proportion of the Mo^{4+} oxidation state increases to 18% at 60 Å. It can be inferred that the oxidation state of Mo^{4+} is mainly reduced from Mo^{5+}.

Figure 5 is the energy level diagram of the Co/MoO_3/BP interface derived from the test data. The WF of the intrinsic BP is 4.24 eV, and the VBM is 0.1 eV. Since the band gap of BP is 0.3 eV, it can be deduced that the conduction band maximum (CBM) is 0.2 eV. The WF of MoO_3 is 6.33 eV and the VBM is 2.72 eV. Since the band gap of MoO_3 is 3.1 eV, the CBM can be deduced to be 0.38 eV. The interface dipole corresponds to the difference between the vacuum levels when the fermi level is the reference energy level, it is found that there is an interface dipole of 2.09 eV at the MoO_3/BP interface, which is oriented from MoO_3 to BP substrate. With the deposition of Co, a chemical reaction occurs at the interface, and MoO_3 is reduced while the WF begins to decrease. After depositing 60 Å of Co, the WF of the sample is 5.24 eV. Since electrons are transferred from Co film to MoO_3, there is an interface dipole from MoO_3 to Co film at the interface, which is 1.09 eV.

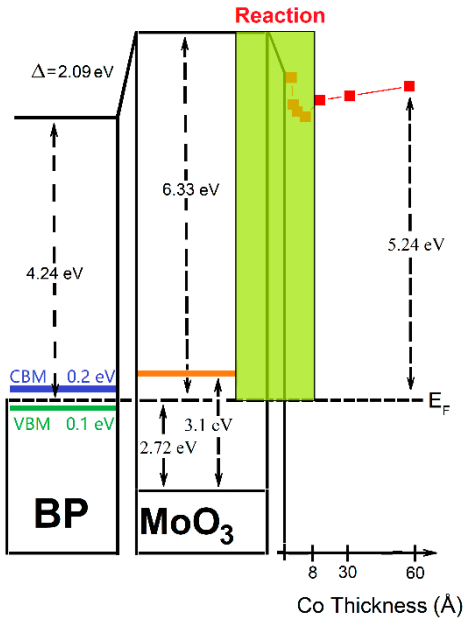

Figure 5. An energy level diagram of the Co/MoO_3/BP interface.

4. Conclusions

In conclusion, the electronic structure of the Co/MoO_3/BP interface was investigated using photoelectron spectroscopy. It was found that a reaction occurred between Co and MoO_3 in the initial deposition stage of Co. Adding a MoO_3 buffer layer between Co and BP effectively prevented the damage to the black phosphorus lattice caused by Co deposition. There was also an interface dipole of 1.09 eV at the Co/MoO_3 interface, and the direction is from MoO_3 to Co film. These research results provide help for the development of spintronic devices based on Co/MoO_3/BP.

Supplementary Materials: The following supporting information can be downloaded at: https://www.mdpi.com/article/10.3390/sym14112448/s1, Table S1: Peak positions and FWHM values of XPS spectra.

Author Contributions: Conceptualization, H.X.; methodology, B.L. and H.X.; software, B.L.; validation, B.L., H.X. and Y.Z.; formal analysis, B.L.; investigation, B.L.; resources, H.X. and D.N.; data curation, B.L.; writing—original draft preparation, B.L.; writing—review and editing, H.X., D.N., and Y.G.; visualization, B.L.; supervision, H.X. and Y.G.; project administration, H.X.; funding acquisition, H.X., D.N. and Y.G. All authors have read and agreed to the published version of the manuscript.

Funding: This research was funded by by the National Natural Science Foundation of China (Grant No. 51802355) and the National Key Research and Development Program of China (Grant No. 2017YFA0206602). H.X. acknowledges the support by the Natural Science Foundation of Hunan Province (Grant No. 2018JJ3625). Y.G. acknowledges the support by the National Science Foundation (Grant No. DMR 1903962).

Data Availability Statement: The data presented in this study are available on request from the corresponding author.

Conflicts of Interest: The authors declare no conflict of interest.

References

1. Zhang, M.; Wu, Q.; Zhang, F.; Chen, L.L.; Jin, X.X.; Hu, Y.W.; Zheng, Z.; Zhang, H. 2d Black Phosphorus Saturable Absorbers for Ultrafast Photonics. *Adv. Opt. Mater.* **2019**, *7*, 1800224. [CrossRef]
2. Liu, H.; Hu, K.; Yan, D.; Chen, R.; Zou, Y.; Liu, H.; Wang, S. Recent Advances on Black Phosphorus for Energy Storage, Catalysis, and Sensor Applications. *Adv. Mater.* **2018**, *30*, e1800295. [CrossRef] [PubMed]
3. Zhao, Y.; Chen, Y.; Zhang, Y.H.; Liu, S.F. Recent Advance in Black Phosphorus: Properties and Applications. *Mater. Chem. Phys.* **2017**, *189*, 215–229. [CrossRef]

4. Ren, X.L.; Lian, P.C.; Xie, D.L.; Yang, Y.; Mei, Y.; Huang, X.R.; Wang, Z.R.; Yin, X.T. Properties, Preparation and Application of Black Phosphorus/Phosphorene for Energy Storage: A Review. *J. Mater. Sci.* **2017**, *52*, 10364–10386. [CrossRef]
5. Lei, W.; Liu, G.; Zhang, J.; Liu, M. Black Phosphorus Nanostructures: Recent Advances in Hybridization, Doping and Functionalization. *Chem. Soc. Rev.* **2017**, *46*, 3492–3509. [CrossRef]
6. Li, L.; Yu, Y.; Ye, G.J.; Ge, Q.; Ou, X.; Wu, H.; Feng, D.; Chen, X.H.; Zhang, Y. Black Phosphorus Field-Effect Transistors. *Nat. Nanotechnol.* **2014**, *9*, 372–377. [CrossRef]
7. Li, L.; Engel, M.; Farmer, D.B.; Han, S.J.; Wong, H.S. High-Performance P-Type Black Phosphorus Transistor with Scandium Contact. *Acs Nano* **2016**, *10*, 4672–4677. [CrossRef]
8. Engel, M.; Steiner, M.; Avouris, P. Black Phosphorus Photodetector for Multispectral, High-Resolution Imaging. *Nano Lett.* **2014**, *14*, 6414–6417. [CrossRef]
9. Youngblood, N.; Chen, C.T.; Koester, S.J.; Li, M. Waveguide-Integrated Black Phosphorus Photodetector with High Responsivity and Low Dark Current. *Nat. Photonics* **2015**, *9*, 247. [CrossRef]
10. Buscema, M.; Groenendijk, D.J.; Steele, G.A.; van der Zant, H.S.; Castellanos-Gomez, A. Photovoltaic Effect in Few-Layer Black Phosphorus Pn Junctions Defined by Local Electrostatic Gating. *Nat. Commun.* **2014**, *5*, 4651. [CrossRef]
11. Dai, J.; Zeng, X.C. Bilayer Phosphorene: Effect of Stacking Order on Bandgap and Its Potential Applications in Thin-Film Solar Cells. *J. Phys. Chem. Lett.* **2014**, *5*, 1289–1293. [CrossRef] [PubMed]
12. Yan, H.G.; Li, X.S.; Chandra, B.; Tulevski, G.; Wu, Y.Q.; Freitag, M.; Zhu, W.J.; Avouris, P.; Xia, F.N. Tunable Infrared Plasmonic Devices Using Graphene/Insulator Stacks. *Nat. Nanotechnol.* **2012**, *7*, 330–334. [CrossRef] [PubMed]
13. Tran, V.; Soklaski, R.; Liang, Y.F.; Yang, L. Layer-Controlled Band Gap and Anisotropic Excitons in Few-Layer Black Phosphorus. *Phys. Rev. B* **2014**, *89*, 235319. [CrossRef]
14. Kou, L.; Frauenheim, T.; Chen, C. Phosphorene as a Superior Gas Sensor: Selective Adsorption and Distinct I-V Response. *J. Phys. Chem. Lett.* **2014**, *5*, 2675–2681. [CrossRef] [PubMed]
15. Sui, X.L.; Si, C.; Shao, B.; Zou, X.L.; Wu, J.; Gu, B.L.; Duan, W.H. Tunable Magnetism in Transition-Metal-Decorated Phosphorene. *J. Phys. Chem. C* **2015**, *119*, 10059–10063. [CrossRef]
16. Kamalakar, M.V.; Madhushankar, B.N.; Dankert, A.; Dash, S.P. Low Schottky Barrier Black Phosphorus Field-Effect Devices with Ferromagnetic Tunnel Contacts. *Small* **2015**, *11*, 2209–2216. [CrossRef]
17. Hong, Q.; Xu, W.; Zhang, J.; Zhu, Z.; Yuan, X.; Qin, S. Optical Activity in Monolayer Black Phosphorus Due to Extrinsic Chirality. *Opt. Lett.* **2019**, *44*, 1774–1777. [CrossRef]
18. Liu, B.; Xie, H.; Wang, S.; Zhao, Y.; Liu, Y.; Niu, D.; Gao, Y. Effect of MoO_3 Buffer Layer on the Electronic Structure of Al–Bp Interface. *J. Phys. D Appl. Phys.* **2022**, *55*, 364005. [CrossRef]
19. Liu, B.X.; Xie, H.P.; Liu, Y.Q.; Wang, C.; Wang, S.T.; Zhao, Y.; Liu, J.X.; Niu, D.M.; Huang, H.; Gao, Y.L. Electronic Structure and Spin Polarization of Co/Black Phosphorus Interface. *J. Magn. Magn. Mater.* **2020**, *499*, 166297. [CrossRef]
20. Liu, B.X.; Xie, H.P.; Niu, D.M.; Huang, H.; Wang, C.; Wang, S.T.; Zhao, Y.; Liu, Y.Q.; Gao, Y.L. Interface Electronic Structure between Au and Black Phosphorus. *J. Phys. Chem. C* **2018**, *122*, 18405–18411. [CrossRef]
21. Sun, G.J.; Shahid, M.; Fei, Z.P.; Xu, S.D.; Eisner, F.D.; Anthopolous, T.D.; McLachlan, M.A.; Heeney, M. Highly-Efficient Semi-Transparent Organic Solar Cells Utilising Non-Fullerene Acceptors with Optimised Multilayer MoO_3/Ag/MoO_3 Electrodes. *Mater. Chem. Front.* **2019**, *3*, 450–455. [CrossRef]
22. Xiang, D.; Han, C.; Wu, J.; Zhong, S.; Liu, Y.; Lin, J.; Zhang, X.A.; Hu, W.P.; Özyilmaz, B.; Neto, A.H.C.; et al. Surface Transfer Doping Induced Effective Modulation on Ambipolar Characteristics of Few-Layer Black Phosphorus. *Nat. Commun.* **2015**, *6*, 6485. [CrossRef] [PubMed]
23. Chu, X.B.; Guan, M.; Zhang, Y.; Li, Y.Y.; Liu, X.F.; Zeng, Y.P. Ito-Free and Air Stable Organic Light-Emitting Diodes Using MoO_3:Ptcda Modified Al as Semitransparent Anode. *RSC Adv.* **2013**, *3*, 9509–9513. [CrossRef]
24. Latif, H.; Zahid, R.; Rasheed, S.; Sattar, A.; Rafique, M.S.; Zaheer, S.; Shabbir, S.A.; Javed, K.; Usman, A.; Amjad, R.J.; et al. Effect of Annealing Temperature of MoO_3 Layer in MoO_3/Au/MoO_3 (Mam) Coated Pbs Qds Sensitized Zno Nanorods/Fto Glass Solar Cell. *Sol. Energy* **2020**, *198*, 529–534. [CrossRef]
25. Wang, F.; Hu, F.; Zhang, X.; Xu, H. In Situ Photoelectron Spectroscopy Investigation of Interface Coupling between Metals and MoO_3 Thin Films. *Surf. Rev. Lett.* **2016**, *24*, 1750042. [CrossRef]
26. Lee, T.H.; Kim, S.Y.; Jang, H.W. Black Phosphorus: Critical Review and Potential for Water Splitting Photocatalyst. *Nanomaterials* **2016**, *6*, 194. [CrossRef]
27. Peelaers, H.; Chabinyc, M.L.; Van de Walle, C.G. Controlling N-Type Doping in MoO_3. *Chem. Mater.* **2017**, *29*, 2563–2567. [CrossRef]
28. Liu, X.L.; Wang, C.G.; Wang, C.C.; Irfan, I.F.; Gao, Y.L. Interfacial Electronic Structures of Buffer-Modified Pentacene/C-60-Based Charge Generation Layer. *Org. Electron.* **2015**, *17*, 325–333. [CrossRef]
29. Biesinger, M.C.; Payne, B.P.; Grosvenor, A.P.; Lau, L.W.M.; Gerson, A.R.; Smart, R.S.C. Resolving Surface Chemical States in Xps Analysis of First Row Transition Metals, Oxides and Hydroxides: Cr, Mn, Fe, Co and Ni. *Appl. Surf. Sci.* **2011**, *257*, 2717–2730. [CrossRef]

30. Biesinger, M.C.; Payne, B.P.; Lau, L.W.M.; Gerson, A.; Smart, R.S.C. X-ray Photoelectron Spectroscopic Chemical State Quantification of Mixed Nickel Metal, Oxide and Hydroxide Systems. *Surf. Interface Anal.* **2009**, *41*, 324–332. [CrossRef]
31. Salaneck, W.R.; Seki, K.; Kahn, A.; Pireaux, J.-J. *Conjugated Polymer and Molecular Interfaces: Science and Technology for Photonic and Optoelectronic Application*; CRC Press: New York, NY, USA, 2001.